

## Temperature-dependent dielectric functions and interband critical points of relaxor lead hafnate-modified $\text{PbSc}_{1/2}\text{Ta}_{1/2}\text{O}_3$ ferroelectric ceramics by spectroscopic ellipsometry

Z. H. Duan, Z. G. Hu, K. Jiang, Y. W. Li, G. S. Wang et al.

Citation: *Appl. Phys. Lett.* **102**, 151908 (2013); doi: 10.1063/1.4802205

View online: <http://dx.doi.org/10.1063/1.4802205>

View Table of Contents: <http://apl.aip.org/resource/1/APPLAB/v102/i15>

Published by the [American Institute of Physics](#).

---

### Additional information on *Appl. Phys. Lett.*

Journal Homepage: <http://apl.aip.org/>

Journal Information: [http://apl.aip.org/about/about\\_the\\_journal](http://apl.aip.org/about/about_the_journal)

Top downloads: [http://apl.aip.org/features/most\\_downloaded](http://apl.aip.org/features/most_downloaded)

Information for Authors: <http://apl.aip.org/authors>

## ADVERTISEMENT



**Goodfellow**  
metals • ceramics • polymers • composites  
70,000 products  
450 different materials  
**small quantities fast**

[www.goodfellowusa.com](http://www.goodfellowusa.com)

# Temperature-dependent dielectric functions and interband critical points of relaxor lead hafnate-modified $\text{PbSc}_{1/2}\text{Ta}_{1/2}\text{O}_3$ ferroelectric ceramics by spectroscopic ellipsometry

Z. H. Duan (段志华),<sup>1</sup> Z. G. Hu (胡志高),<sup>1,a)</sup> K. Jiang (姜凯),<sup>1</sup> Y. W. Li (李亚巍),<sup>1</sup> G. S. Wang (王根水),<sup>2</sup> X. L. Dong (董显林),<sup>2</sup> and J. H. Chu (褚君浩)<sup>1</sup>

<sup>1</sup>Key Laboratory of Polar Materials and Devices, Ministry of Education, Department of Electronic Engineering, East China Normal University, Shanghai 200241, China

<sup>2</sup>Key Laboratory of Inorganic Functional Materials and Devices, Shanghai Institute of Ceramics, Chinese Academy of Sciences, Shanghai 200050, China

(Received 7 December 2012; accepted 4 April 2013; published online 16 April 2013)

The electronic band structures and dielectric functions of  $(1-x)\text{PbSc}_{1/2}\text{Ta}_{1/2}\text{O}_3-x\text{PbHfO}_3$  ceramics with different composition have been investigated by variable-temperature spectroscopic ellipsometry. Using the standard critical-point (SCP) model, three typical interband transitions can be observed from the second derivative of dielectric functions. The CP transitions, which are sensitive to B-site order degree, show a redshift trend with the temperature due to the electron-phonon interactions and lattice thermal expansion. The linear temperature coefficients are varied with oxygen vacancy, B-atom (Sc, Ta, Hf) arrangement, and Pb-O bonds owing to addition of  $\text{PbHfO}_3$ .  
 © 2013 AIP Publishing LLC [<http://dx.doi.org/10.1063/1.4802205>]

Relaxor ferroelectrics are extensively studied due to their excellent dielectric, electrostrictive, and pyroelectric properties and accordingly their applications in tunable capacitors, actuators, and electro-optic devices.<sup>1–6</sup> In particular, Pb-based  $\text{ABO}_3$  perovskites have attracted considerable attention, such as  $\text{PbMg}_{1/3}\text{Nb}_{2/3}\text{O}_3$  (PMN),  $\text{PbFe}_{1/2}\text{Nb}_{1/2}\text{O}_3$  (PFN),  $\text{PbFe}_{1/2}\text{Ta}_{1/2}\text{O}_3$  (PFT), and  $\text{PbSc}_{1/2}\text{Ta}_{1/2}\text{O}_3$  (PST).<sup>1,6–8</sup> In this kind of compounds, the Pb off shifts are essential for the occurrence of spontaneous polarization. Both Pb-O and B-O hybridizations are important in polar instabilities, indicating the complexity of physical mechanism for these materials.<sup>1,4</sup> Among them, PST is of high interest due to its high permittivity with a broad maximum near room temperature. From the structural point of view,  $\text{Sc}^{3+}$  and  $\text{Ta}^{5+}$  cations may occupy B sites randomly or can develop 1:1 NaCl-type order on the {111} planes. Note that the arrangement of cations can be described by the B-site order degree.<sup>3,8</sup> It is well-known that the B-site order plays an important role in the physical properties, including phase transition temperature, dielectric response, and electronic interband transitions.<sup>5,8,9</sup> Correspondingly, the structural order can be controlled by the doping/mixing or growth parameters, such as thermal treatment. Thus, macroscopical physical properties derived by these factors should be thoroughly studied by means of electrical, optical, and magnetic measurements.

Especially, several interesting solid solutions of PST-based perovskites, such as  $(1-x)\text{PbSc}_{1/2}\text{Ta}_{1/2}\text{O}_3-x\text{PbTiO}_3$  and  $(1-x)\text{PbSc}_{1/2}\text{Ta}_{1/2}\text{O}_3-x\text{PbZrO}_3$ , present improved dielectric and pyroelectric properties.<sup>10,11</sup> Although mixing PST system with  $\text{PbHfO}_3$  [ $(1-x)\text{PbSc}_{1/2}\text{Ta}_{1/2}\text{O}_3-x\text{PbHfO}_3$ , (PSTH)] can increase Curie temperature ( $T_c$ ), decrease sintering temperature, tailor the B-site order, and enhance pyroelectric properties of PST ceramics,<sup>9</sup> the intrinsic mechanism and

its origin have not been presented to date. Recently, we have studied the electronic band structures and dielectric functions of PSTH ceramics by reflectance spectra at room temperature. It was found that the electronic structures, which depend closely on the  $\text{BO}_6$  octahedron, are sensitive to the B-site atom concentration.<sup>8</sup> Unfortunately, temperature effect on the electronic band structures, which can give an important insight on the pyroelectric, ferroelectric, and dielectric properties of ferroelectric oxides, is still an open issue. Therefore, physical mechanism behind the phenomena needs further investigations with aid of spectral experiments under different external fields (such as temperature and pressure), which can induce the structural and electronic state variations.

On the other hand, dielectric functions ( $\epsilon$ ) are crucial for the design and optimization of optoelectronic devices. The parameters  $\epsilon$  exhibit numerous peak or shoulder structures, which are closely associated with electronic transitions. It was reported that the dielectric behavior of  $\text{Pb}(\text{B}_1\text{B}_2)\text{O}_3$  is related to the nature of chemical distribution for B-site cations on the octahedral sublattice.<sup>2</sup> Fortunately, the dielectric functions of semiconductors and/or ferroelectric materials can be measured by spectroscopic ellipsometry (SE), which also give the information about microstructure and electronic band structure.<sup>12–14</sup> In addition, it can be used to study the band and local (corrected) character in the optical spectra of solids.<sup>13</sup> Moreover, temperature-dependence of interband electronic transition energies can provide important information about collective excitations and absorption characteristics. Therefore, variable-temperature SE analysis is desirable for presenting more insights on the intrinsic features for optical response behavior of PSTH ferroelectric oxides.

In this letter, temperature dependence of dielectric functions and interband critical-point parameters of PSTH ceramics have been investigated by spectroscopic ellipsometry. Influences from the temperature and  $\text{PbHfO}_3$  composition on electronic band structure have been discussed in detail.

<sup>a)</sup> Author to whom correspondence should be addressed. Electronic mail: [zghu@ee.ecnu.edu.cn](mailto:zghu@ee.ecnu.edu.cn). Tel.: +86-21-54345150. Fax: +86-21-54345119.

The PSTH powders ( $x = 0, 0.05, 0.1, 0.15,$  and  $0.2$ ) were synthesized by the two-stage calcination route and the ceramics were fabricated by hot-pressing sintering method. Note that 5 wt. % excess PbO was added to compensate for the PbO loss during sintering.<sup>8,9</sup> All PSTH ceramic wafers were double-side polished with a mechanical polishing process to smooth the surface. This process consists of three procedures: coarse grinding, fine grinding, and polishing. Then, the ceramics were rigorously cleaned in pure ethanol with an ultrasonic bath and rinsed several times by deionized water for spectral measurements. The X-ray diffraction (XRD) pattern shows that the ceramics are well crystallized in perovskite structure without the impurity phases.<sup>9</sup> From the XRD and infrared reflectance spectra, the degree of structure ordering on B-site was calculated. A variable structural ordering was found in PSTH solid solutions where the B-site order decreases by increasing PbHfO<sub>3</sub> composition ( $0 \leq x \leq 0.1$ ) and becomes completely disordered ( $x = 0.1, 0.15,$  and  $0.2$ ).<sup>8,9</sup> Temperature-dependent SE experiments were carried out in the photon energy range of 1.24–6.4 eV (193–1000 nm) by a vertical variable-angle near-infrared-ultraviolet SE (V-VASE by J.A. Woollam Co., Inc.). It was measured with the zone average polarizer at an incident angle of 70° and the spectral interval is set to 2 nm. For the variable-temperature measurements, the samples are mounted into a Instec cell and the temperature can be controlled from –60 to 400 °C with a precision of about  $\pm 1$  °C. Note that the surface roughness can be neglected in extracting the dielectric function because the root-mean-square roughness is about 2 nm, which can be derived from atomic force microscopy (AFM) experiment (Bruker Dimension Icon). It indicates that the present ceramics are free from surface oxidation due to the fact that the severely polishing treatment is taken.

Figures 1(a)–1(e) show the real and imaginary parts of dielectric functions ( $\epsilon = \epsilon_1 + i\epsilon_2$ ) for PSTH ( $0 \leq x \leq 0.2$ ) ceramics between 1.24 and 6.4 eV at –60, 100, 200, 400 °C, respectively. The  $\epsilon$  of all PSTH ceramics shows the similar behaviors with increasing the temperature, which has an obvious effect on the dielectric functions. From the change of  $\epsilon_2$ , it is evident that the intensity of peak located around 3.75 eV decreases with increasing the temperature, while the peak around 5.35 eV shows an opposite trend. Especially, the amplitude variation of the transition peak around 5.35 eV is distinct, as shown in Figure 1(f). The peaks and shoulder structures in the  $\epsilon_2$  spectra correspond to  $p$ - $d$  and  $d$ - $d$  charge-transfer transitions or the electronic band-band transitions.<sup>15</sup> Note that the intensity of peaks is also sensitive to the interband transitions. As the temperature increases, the  $\epsilon_{2max}$  decreases slightly first and then increases gradually. Note that the value keeps almost unchanged in the high temperature ( $> 200$  °C) region. The parameter  $\epsilon_{2max}$  has the minimal value around  $T_c$  and it may be due to the structure transformation from cubic (paraelectric) to rhombohedral (ferroelectric) at  $T_c$ , which was confirmed by temperature-dependent Raman scattering experiments.<sup>5</sup> The conversion from increment to near constant appears around 200 °C, which can be ascribed to the stabilization by the tetragonal strain and enhanced correlations between polar nanoregions or associated with the occurrence of polar-cluster coupling.<sup>4,5</sup> Note

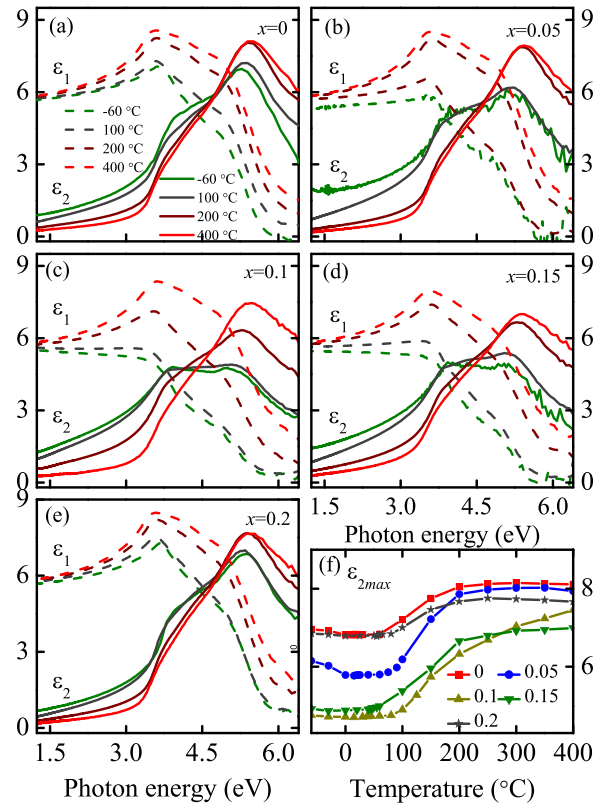


FIG. 1. (a)–(e) Real ( $\epsilon_1$ ) and imaginary ( $\epsilon_2$ ) parts of dielectric functions for  $(1-x)\text{PbSc}_{1/2}\text{Ta}_{1/2}\text{O}_3-x\text{PbHfO}_3$  ceramics measured at –60, 100, 200, and 400 °C, respectively. (f) The maximum value of  $\epsilon_2$  as a function of the temperature from –60 to 400 °C for PSTH ceramics.

that the PST ceramic (i.e.,  $x = 0$ ) has the maximal value of dielectric function in the entire temperature range. The  $\epsilon_{2max}$  decreases with increasing  $x$  ( $x = 0, 0.05,$  and  $0.1$ ). For the disordered PSTH ( $x = 0.1, 0.15,$  and  $0.2$ ) ceramics, however, the  $\epsilon_{2max}$  becomes larger with increased PbHfO<sub>3</sub> composition. It was found that the B-site order decreases with addition of PbHfO<sub>3</sub> ( $x = 0, 0.05, 0.1$ ) from XRD and infrared reflectance.<sup>8,9</sup> The B-site atom arrangement can be related to the electronic band structures and then influence the  $\epsilon_{2max}$ .<sup>16,17</sup> When  $x$  is larger than 0.05, however, the PSTH ceramics become completely disordered and the lattice expands with increasing  $x$ .<sup>9</sup> The lattice expansion and oxygen vacancies mostly affect the formation of band structures and induce the increment of  $\epsilon_{2max}$ .<sup>18</sup> The results agree well with the previous reports derived by ultraviolet-near-infrared reflectance spectra at room temperature.<sup>8</sup>

In order to further analyze the fine band structures of  $\epsilon$ , which correspond to the interband transitions (critical points, CPs), the second derivative of dielectric functions ( $d^2\epsilon/dE^2$ ) is calculated. A line-shape analysis with standard critical-point (SCP) model was performed, which has been applied to semiconductors and ferroelectric materials.<sup>19,20</sup> The SCP expression can be written as the following:<sup>13</sup>

$$\frac{d^2\epsilon}{dE^2} = \begin{cases} n(n-1)A_m e^{i\phi_m} (E - E_m + i\Gamma_m)^{n-2}, & n \neq 0 \\ A_m e^{i\phi_m} (E - E_m + i\Gamma_m)^{-2}, & n = 0. \end{cases} \quad (1)$$

Here,  $A_m$ ,  $E_m$ ,  $\Gamma_m$ , and  $\phi_m$  in order are the  $m$ th amplitude, threshold energy, broadening, and excitonic phase angle,

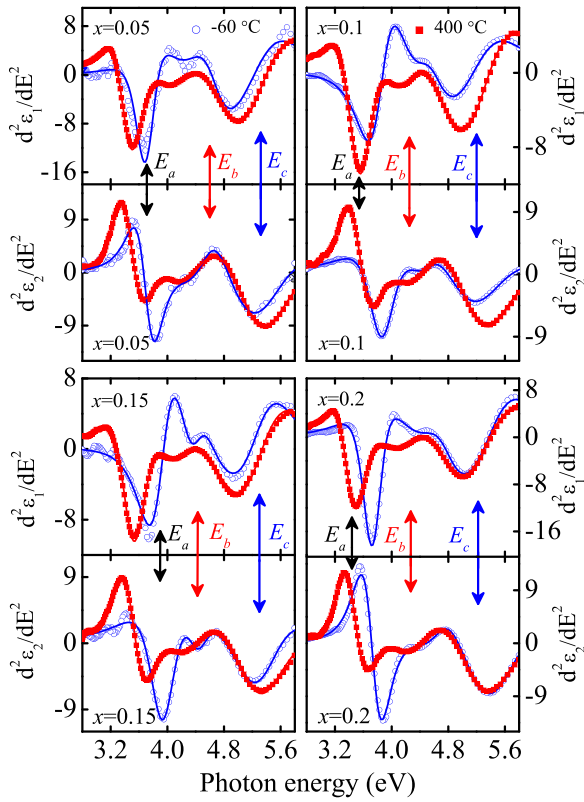


FIG. 2. Experimental (dots) and the best-fit (solid lines) second derivatives of  $\epsilon_1$  and  $\epsilon_2$  at  $-60$  and  $400$  °C for PSTH ( $x=0.05, 0.1, 0.15,$  and  $0.2$ ) ceramics, respectively. Note that the arrows indicate three typical interband electronic transitions.

respectively. The exponent  $n$  has the value of  $-\frac{1}{2}, 0, \frac{1}{2}$ , and  $-1$ , which corresponds to the one-dimensional (1D), 2D, 3D, and excitonic CPs, respectively. For example, Figure 2 displays the experimental and best-fit second derivatives of dielectric functions at  $-60$  and  $400$  °C for PSTH ( $x=0.05, 0.1, 0.15,$  and  $0.2$ ) ceramics. Three interband transitions can be observed clearly and the CPs are labeled as  $E_a, E_b,$  and  $E_c$  in the order of increasing the photon energy. Based on the

simulation, the parameter values of SCP model are listed in Table I. The error bars are less than  $0.02$  eV for the parameter  $A_0$  ( $A_1$ ) and  $0.15$  eV for  $A_2$ . As for the phase angle  $\phi_m$  ( $m=0, 1, 2$ ) and broadening  $\Gamma_m$  ( $m=0, 1, 2$ ), the error bars are less than  $0.9^\circ$  and  $0.01$  eV, respectively. According to the fitting values, the CP energies are estimated to be  $3.72 \pm 0.08, 4.81 \pm 0.11,$  and  $5.39 \pm 0.12$  eV for PST ( $x=0$ ) ceramic at  $-60$  °C. The phase angle  $\phi$  of three CPs is located between  $0^\circ$  and  $90^\circ$ , which describes the excitonic metamorphism of critical-point line shapes.<sup>13</sup>

The interband transitions of perovskite oxides play a crucial role in studying the electronic band structures.<sup>12,17</sup> The key step will find the relationship between the band-to-band transition and microscopic electronic structure. It can be well fulfilled by assigning the interband transition origins. For  $ABO_3$  perovskite, the  $BO_6$  octahedron governs the low-lying conduction band (CB) and the valence band (VB) maximum. However, when A-site is occupied by Pb atoms, the Pb  $6s^2p^2$  plays an important role in the band structures (i.e., PMN and PFT).<sup>1,6</sup> As an example, Lampis *et al.* calculated the electronic structure of PFT theoretically and it was found that the VB mainly consists of O  $2p$  states and Pb  $6s$  states while CB is dominated by Fe  $3d, Ta 5d,$  and Pb  $6p$  states.<sup>6</sup> Base on the theoretical electronic band structures of PZT, PMN, PFT, and  $Ba_2ScTaO_6$  oxides,<sup>1,6,12,21,22</sup> it was concluded that the O  $2p$  states mainly dominate the VBM and the CB consists of Sc(Ta)  $d$  states and Pb  $6p$  states for the PST ceramics. Similar to the  $PbHfO_3,$  Pb-O bonding can also make contributions to the band structures of PSTH ceramics.<sup>8,22</sup> Note that the CP  $E_b$  cannot be distinguished from reflectance spectra due to the weak intensity.<sup>8</sup> However, it can be clearly observed from the second derivatives of dielectric functions determined by SE spectra, as shown in Figure 2. The transition energy  $E_a$  corresponds to the transitions from O  $2p$  to the B-site  $d$  states [Sc  $3d$  and Ta (Hf)  $5d$ ] states. The transition energy  $E_c$  may be attributed to transitions from the O  $2p$  to Pb  $6p$  states and/or the hybridized states with B-site  $d$  states. The assignment of transition

TABLE I. The SCP model parameters for  $(1-x)PbSc_{1/2}Ta_{1/2}O_3-xPbHfO_3$  ceramics are extracted from the best fitting second derivatives of dielectric functions (Fig. 2) at  $-60, 200,$  and  $400$  °C, respectively.

Samples $x$	Temperature (°C)	$E_a$				$E_b$				$E_c$			
		$A_0$ (eV)	$\phi_0$ (deg)	$E_0$ (eV)	$\Gamma_0$ (eV)	$A_1$ (eV)	$\phi_1$ (deg)	$E_1$ (eV)	$\Gamma_1$ (eV)	$A_2$ (eV)	$\phi_2$ (deg)	$E_2$ (eV)	$\Gamma_2$ (eV)
0	-60	1.32	45.0	3.72	0.34	1.41	49.5	4.81	0.51	10.3	40.4	5.39	0.92
	200	0.97	44.6	3.56	0.29	0.59	46.9	4.43	0.40	7.62	39.8	5.34	0.73
	400	0.87	44.5	3.49	0.28	0.94	46.1	4.21	0.49	7.67	39.6	5.29	0.77
0.05	-60	0.88	45.2	3.72	0.30	1.13	48.9	4.62	0.47	6.48	40.6	5.33	0.88
	200	1.08	44.5	3.56	0.32	0.60	46.9	4.44	0.45	7.37	39.8	5.32	0.76
	400	1.04	44.3	3.46	0.33	0.96	46.4	4.27	0.53	8.10	39.6	5.25	0.82
0.1	-60	1.27	46.3	3.86	0.40	0.31	48.0	4.55	0.40	4.49	40.3	5.21	0.88
	200	1.26	45.3	3.66	0.37	0.66	46.0	4.31	0.51	4.42	39.9	5.28	0.76
	400	1.10	44.6	3.54	0.36	0.99	46.1	4.25	0.55	6.74	39.4	5.20	0.82
0.15	-60	1.52	46.3	3.93	0.40	0.23	46.3	4.43	0.31	3.38	40.5	5.31	0.70
	200	1.14	45.0	3.64	0.36	0.34	46.1	4.33	0.40	4.98	39.9	5.29	0.77
	400	1.10	44.6	3.52	0.36	0.52	46.0	4.23	0.47	5.03	39.7	5.26	0.77
0.2	-60	1.19	45.0	3.74	0.30	0.61	48.6	4.73	0.45	7.15	40.2	5.41	0.82
	200	1.00	44.5	3.54	0.31	0.76	46.7	4.40	0.49	7.01	39.8	5.31	0.77
	400	0.97	44.3	3.44	0.32	1.30	46.3	4.27	0.60	7.10	39.5	5.22	0.80

energy  $E_b$  located between  $E_a$  and  $E_c$  is complicated because it may be related to both B-site  $d$  states and Pb  $6p$  states. For the  $\text{Pb}(\text{Zr}_x\text{Ti}_{1-x})\text{O}_3$  ( $x = 0.2, 0.56, \text{ and } 0.82$ ) films, there also exists three CPs (3.9, 4.5, and 6.5 eV) at room temperature.<sup>12</sup> The discrepancy between the transition energy can be attributed to the effective electronegativity of B-site atoms and CB width influenced by B-O-B bonds.<sup>21</sup> It should be emphasized that the distinct variation appears between the spectra recorded at  $-60$  and  $400^\circ\text{C}$ , especially near the CP  $E_a$  ( $\sim 3.7$  eV), which indicates that the temperature has a remarkable influence on electronic band structures of PSTH ceramics.

In order to make further investigation about the interband transition, the temperature dependence of the interband critical point energies of PSTH ceramics is presented in Figures 3(a)–3(e). Correspondingly, Figure 3(f) shows the amplitude variation of  $E_a$  and  $E_c$  with the temperature for PSTH ceramic ( $x = 0.1$ ). It indicates that the amplitude of  $E_a$  decreases with the temperature while the intensity of  $E_c$  is enhanced, which is consistent with the experimental results as shown in Figure 1(f). As for the variation of excitonic phase angle, it was found that the deviation of  $\phi$  between  $-60$  and  $400^\circ\text{C}$  is less than  $2^\circ$  for the CPs from Table I. Actually, the angle almost keeps constancy with increasing the temperature, which confirms the correctness of the line-shape chosen for those CPs. The three interband transition energies show a red-shift trend with increasing the

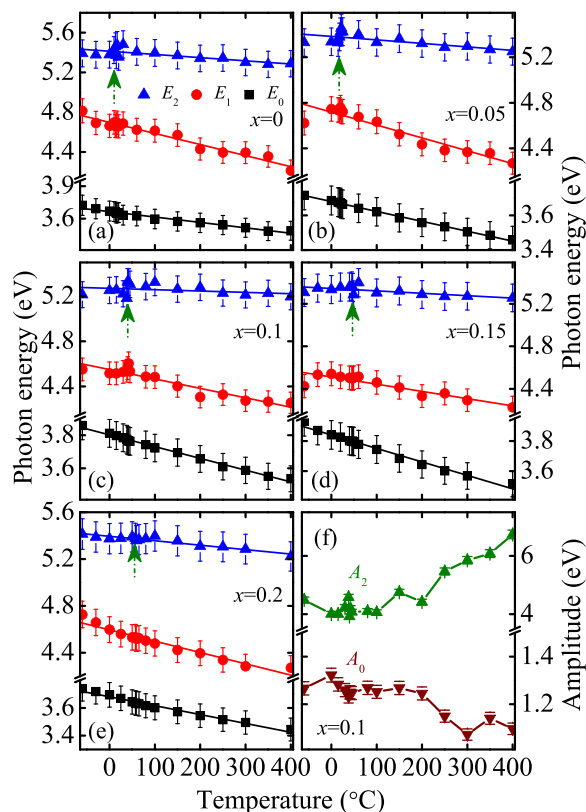


FIG. 3. (a)–(e) Temperature dependence of the interband critical point energies for PSTH ceramics. The solid lines represent the linear fitting results to guide the eyes. (f) The amplitude of CPs  $E_a$  and  $E_c$  variation with the temperature for  $(1-x)\text{PbSc}_{1/2}\text{Ta}_{1/2}\text{O}_3-x\text{PbHfO}_3$  ( $x = 0.1$ ) ceramics. Note that the arrows indicate the small jump in the CP  $E_c$ , which corresponds to Curie temperature.

temperature, which is similar to that of silicon, GaAs, and  $0.76\text{Pb}(\text{Mg}_{1/3}\text{Nb}_{2/3})\text{O}_3-0.24\text{PbTiO}_3$  single crystal.<sup>13,23</sup> The negative temperature dependence of the transition energy can be explained by the renormalization of the band structures caused by electron-phonon interaction and lattice thermal expansion. To investigate the behaviors of the CPs with the temperature, the transition energies can be fitted by the linear function:  $E(T) = E_0 - \lambda_i T$  ( $i$  means the  $i$ th CP), which is shown by the solid lines in Figures 3(a)–3(e). For PSTH ( $x = 0.1$ ) ceramic, the linear temperature coefficients  $\lambda_1$ ,  $\lambda_2$ , and  $\lambda_3$  are  $7.1 \times 10^{-4}$ ,  $8.4 \times 10^{-4}$ , and  $1.2 \times 10^{-4}$  eV/ $^\circ\text{C}$ , respectively. The parameters can be comparable with the data from semiconductor silicon ( $4.1 \times 10^{-4}$  eV/K).<sup>13</sup> The highest electronic transition shows the minimal variation for PSTH ceramic, which indicates that the temperature has minimal influence on the CP  $E_c$ . For the first CP, the  $\lambda_1$  is estimated to be  $(5.0 \pm 0.2) \times 10^{-4}$ ,  $(5.7 \pm 0.1) \times 10^{-4}$ ,  $(7.1 \pm 0.2) \times 10^{-4}$ ,  $(8.9 \pm 0.4) \times 10^{-4}$ , and  $(6.4 \pm 0.3) \times 10^{-4}$  eV/ $^\circ\text{C}$  with increasing  $\text{PbHfO}_3$  composition, suggesting that the coefficient of  $E_a$  becomes larger with addition of  $\text{PbHfO}_3$ . However, when the  $x$  is larger than 0.15, the coefficient  $\lambda_1$  decreases. For the second CP  $E_b$ , the linear coefficient  $\lambda_2$  is estimated to be  $1 \times 10^{-3}$ ,  $1 \times 10^{-3}$ ,  $8.4 \times 10^{-4}$ ,  $6.8 \times 10^{-4}$ ,  $9.8 \times 10^{-4}$  eV/ $^\circ\text{C}$ . Correspondingly, the parameter  $\lambda_3$  is  $3.2 \times 10^{-4}$ ,  $2.7 \times 10^{-4}$ ,  $1.2 \times 10^{-4}$ ,  $2.3 \times 10^{-4}$ , and  $3.6 \times 10^{-4}$  eV/ $^\circ\text{C}$ . Both  $\lambda_2$  and  $\lambda_3$  values become smaller first and then increase with increasing  $\text{PbHfO}_3$  composition. It should be noted that the standard errors of these coefficients are much less than  $5 \times 10^{-5}$  eV/ $^\circ\text{C}$ , which indicates that the linear analysis can be acceptable and reasonably describe the variation trends.

It was found that PSTH ( $x = 0.15$ ) ceramic shows the largest value of  $\lambda_1$ , which could be explained by the largest lattice expansion resulted from the  $\text{Hf}^{4+}$  occupation into the B-site. For PSTH ceramics ( $0 < x \leq 0.15$ ), the B-site average radius and lattice constants increase. Due to addition of  $\text{PbHfO}_3$ , the oxygen vacancy forms to make balance of charge and the concentration increases with increasing  $x$ .<sup>9</sup> Nevertheless, the  $\text{Hf}^{4+}$  ions prefer to replace the  $\text{Sc}^{3+}$  ions and subsequently produces Pb vacancy for  $x = 0.2$ .<sup>9</sup> In addition, the incorporation of  $\text{PbHfO}_3$  reduces the B-site ordering and forms the Hf-O-Hf and Ta-O-Hf chains, which can also affect the variation of electronic transition energy. Moreover, the oxygen vacancy located between B-cations and the B-cation arrangement plays an important role in band-structure engineering for perovskite  $\text{ABB}'\text{O}_3$  solid solutions.<sup>18</sup> Especially, for the Pb-based compounds, the formation of short Pb-O bonds and electrostatic interaction among B-site atoms will also influence the dielectric properties.<sup>24</sup> For PSTH ( $x = 0.2$ ) ceramic, the existence of Pb vacancy has an effect on the Pb-O bonds and repulsive interaction between B-atoms  $d$  states. From high-temperature Raman scattering, it was also concluded that the length of coherence within the Pb-O system can affect the strength of coupling between spatial polar regions comprising off-centered B cations.<sup>4</sup> For the second CP, the  $\lambda_2$  shows the similar variation to  $\lambda_3$  and a completely reverse trend of  $\lambda_1$ . It has the minimal value at  $x = 0.15$ , which can be also related to the oxygen vacancy and lattice expansion. It indicates that the composition has a remarkable influence on interband transitions. This

phenomenon also reflects the complexity of interband transition  $E_b$  and multiple transitions will happen at the same peak position.<sup>17</sup> As for the last critical point  $E_c$ , the variation trend of  $\lambda_3$  is correlated with the B-site order degree and has the minimal value at  $x = 0.1$ . As shown in Figure 1(f), the interband transition located around 5.3 eV is sensitive to the structural order parameters induced by mixing with PbHfO<sub>3</sub>. It should be noted that the transition energy  $E_c$  shows a little jump around the  $T_c$  (marked by the arrows) due to the structural variation. Since the CP  $E_c$  corresponds to the transition between O  $2p$  and Pb  $6p$  states (hybridization with B-site  $d$ ), it is concluded that the structural transformation is sensitive to the Pb atoms. In addition, the polarizable long pair in the  $6s$  state of Pb<sup>2+</sup> is related to the ferroelectric behavior.<sup>25</sup> Therefore, the Pb<sup>2+</sup> ions and BO<sub>6</sub> (B = Sc, Ta, and Hf) octahedron dominate the electronic band structures (i.e., the interband transitions) of PSTH ceramics. Thus, the different temperature coefficients of CPs can be related to lattice expansion, existence of oxygen vacancy, and B-site order degree induced by addition of PbHfO<sub>3</sub>.

In summary, the temperature and composition dependence of the dielectric functions and electronic band transitions of PSTH ceramics have been investigated using spectroscopy ellipsometry. The three interband transitions show a red-shift pattern with increasing the temperature due to the lattice thermal expansion and electron-phonon interaction in the temperature range of  $-60$ – $400$  °C. The addition of PbHfO<sub>3</sub> results in the occurrence of oxygen vacancy, lattice expansion, and degradedness of B-site order, which can contribute to the variation of electronic band structures.

One of the authors (Z.H.D.) would like to thank Ting Huang for AFM measurements. This work was financially supported by Major State Basic Research Development Program of China (Grant Nos. 2011CB922200 and 2013CB922300), Natural Science Foundation of China (Grant Nos. 11074076, 60906046, and 61106122), Project of Science and Technology Commission of Shanghai Municipality (Grant No. 11520701300), and the Program for

Professor of Special Appointment (Eastern Scholar) at Shanghai Institutions of Higher Learning.

- <sup>1</sup>M. Suewattana and D. J. Singh, *Phys. Rev. B* **73**, 224105 (2006).
- <sup>2</sup>Y. Park, K. M. Knowles, and K. Cho, *J. Appl. Phys.* **83**, 5702 (1998).
- <sup>3</sup>J. Petzelt, E. Buixaderas, and A. V. Pronin, *Mater. Sci. Eng. B* **55**, 86 (1998).
- <sup>4</sup>B. Mihailova, B. Maier, C. Paulmann, T. Malcherek, J. Ihringer, M. Gospodinov, R. Stosch, B. Güttler, and U. Bismayer, *Phys. Rev. B* **77**, 174106 (2008).
- <sup>5</sup>W. J. Zhang, W. W. Li, X. G. Chen, Z. G. Hu, W. Liu, G. S. Wang, X. L. Dong, and J. H. Chu, *Appl. Phys. Lett.* **99**, 041902 (2011).
- <sup>6</sup>N. Lampis, C. Franchini, G. Satta, A. G.-Lehmann, and S. Massidda, *Phys. Rev. B* **69**, 064412 (2004).
- <sup>7</sup>M. Correa, A. Kumar, S. Priya, R. S. Katiyar, and J. F. Scott, *Phys. Rev. B* **83**, 014302 (2011).
- <sup>8</sup>W. J. Zhang, Z. H. Duan, K. Jiang, Z. G. Hu, G. S. Wang, X. L. Dong, and J. H. Chu, *Acta Mater.* **60**, 6175 (2012).
- <sup>9</sup>W. Liu, G. S. Wang, S. Cao, C. L. Mao, F. Cao, and X. L. Dong, *J. Am. Ceram. Soc.* **93**, 2735 (2010); **93**, 3023 (2010).
- <sup>10</sup>P. C. Osbond and R. W. Whatmore, *J. Mater. Sci.* **28**, 1377 (1993).
- <sup>11</sup>J. R. Giniewicz, A. S. Bhalla, and L. E. Cross, *Ferroelectrics* **118**, 157 (1991).
- <sup>12</sup>H. Lee, Y. S. Kang, S.-J. Cho, B. Xiao, H. Morkoç, T. D. Kang, G. S. Lee, J. Li, S.-H. Wei, P. G. Snyder, and J. T. Evans, *J. Appl. Phys.* **98**, 094108 (2005).
- <sup>13</sup>P. Lautenschlager, M. Garriga, L. Viña, and M. Cardona, *Phys. Rev. B* **35**, 9174 (1987); **36**, 4821 (1987).
- <sup>14</sup>N. N. Kovaleva, A. V. Boris, P. Yordanov, A. Maljuk, E. Brücher, J. Stempfer, M. Konuma, I. Zegkinoglou, C. Bernhard, A. M. Stoneham, and B. Keimer, *Phys. Rev. B* **76**, 155125 (2007).
- <sup>15</sup>S. G. Choi, H. T. Yi, S.-W. Cheong, J. N. Hilfiker, R. France, and A. G. Norman, *Phys. Rev. B* **83**, 100101(R) (2011).
- <sup>16</sup>T. N. Stanislavchuk, A. A. Sirenko, A. P. Litvinchuk, X. Luo, and S.-W. Cheong, *J. Appl. Phys.* **112**, 044108 (2012).
- <sup>17</sup>Y. Q. Shen and Z. X. Zhou, *J. Appl. Phys.* **103**, 074113 (2008).
- <sup>18</sup>T. Qi, M. T. Curnan, S. Kim, J. W. Bennett, I. Grinberg, and A. M. Rappe, *Phys. Rev. B* **84**, 245206 (2011).
- <sup>19</sup>H. Lee, Y. S. Kang, S.-J. Cho, B. Xiao, H. Morkoç, and T. D. Kang, *Appl. Phys. Lett.* **86**, 262902 (2005).
- <sup>20</sup>S. G. Choi, H. Y. Zhao, C. Persson, C. L. Perkins, A. L. Donohue, B. To, A. G. Norman, J. Li, and I. L. Repins, *J. Appl. Phys.* **111**, 033506 (2012).
- <sup>21</sup>H. W. Eng, P. W. Barnes, B. M. Auer, and P. M. Woodward, *J. Solid State Chem.* **175**, 94 (2003).
- <sup>22</sup>M. Kitamura and H. Chen, *Ferroelectrics* **210**, 13 (1998).
- <sup>23</sup>J. J. Zhu, W. W. Li, G. S. Xu, K. Jiang, Z. G. Hu, M. Zhu, and J. H. Chu, *Appl. Phys. Lett.* **98**, 091913 (2011).
- <sup>24</sup>L. Bellaiche, J. Padilla, and D. Vanderbilt, *Phys. Rev. B* **59**, 1834 (1999).
- <sup>25</sup>S. V. Halilov, M. Fornari, and D. J. Singh, *Phys. Rev. B* **69**, 174107 (2004).